Available online at www.sciencedirect.com
SCIENCE DIRECT®
Journal of Nuclear Materials 320 (2003) 272–279
journal of nuclear materials
www.elsevier.com/locate/jnucmat

Effects of hydrogen content and temperature on fracture toughness of Zircaloy-4

G. Bertolino [a,*], G. Meyer [a,b], J. Perez Ipiña [b,c]

[a] Centro Atómico Bariloche, CNEA, (8400) Bariloche, Argentina
[b] CONICET, Argentina
[c] Universidad Nacional del Comahue, (8300) Neuquén, Argentina

Received 22 October 2002; accepted 13 March 2003

Abstract

The influence of hydrogen content and temperature on the fracture toughness of a Zircaloy-4 commercial alloy was studied in this work. Toughness was measured on CT specimens obtained from a rolled material. The analysis was performed in terms of J-integral resistance curves. The specimens were fatigue pre-cracked and hydrogen charged before testing them at different temperatures in the range of 293–473 K. A negative influence of the H content on material toughness was important even at very small concentrations, being partially restored when the test temperature increased. Except for some specimens with high H concentration tested at room temperature, the macroscopic fracture behaviour was ductile. The role of Zr-hydrides and $Zr(Fe,Cr)_2$ precipitates in the crack growth and the dependence with hydrogen content were analysed by observation of the fracture surfaces and determination of the $Zr(Fe,Cr)_2$ precipitates density on them.

1. Introduction

It has long been known that zirconium-based cladding alloys absorb hydrogen (H) as a result of service in a nuclear reactor environment. This hydrogen can be absorbed from different potential sources: H cathodically generated as a result of the corrosion of the cladding by the primary side water coolant [1], H gas dissolved in the primary side coolants in pressurized water reactors [2] and hydrogen resulting from corrosion by gases or vapours containing H in the internal plenum region of the rods [3].

Different stable phases are present in the zirconium–hydrogen (Zr–H) system, depending on the H content and temperature. For temperatures below 773 K these equilibrium phases are [4]:

- αZr, with H in solid solution in the matrix,
- δ hydride, $ZrH_{1.5}$ to $ZrH_{1.66}$, with a fcc structure which initially precipitates as platelets in αZr,
- ε hydride, $ZrH_{1.66}$ to ZrH_2, fct, which comes from a martensitic transformation of δ.

Since Zircaloy-4 [1] (Zry-4) is 98% Zr, the Zr–H phase diagram is employed when the H–Zry-4 interaction is studied, although this consideration does not account for the influence of alloying elements on the H absorption process. These alloying elements are present in solid

* Corresponding author. Present address: LMS, UMR-CNRS, Ecole Polytechnique, 91128 Palaiseau cedex, France. Tel.: +33-169 333305; fax: +33-169 333507.
E-mail addresses: bertolin@cab.cnea.gov.ar, bertolin@lms.polytechnique.fr (G. Bertolino).

[1] ZIRCALOY is a trademark of Westinghouse Electric Company, USA.

0022-3115/03/$ - see front matter
doi:10.1016/S0022-3115(03)00193-4

solution in the Zr matrix, or as second phase precipitates preferentially located in the grain boundaries. When hydrogen is absorbed into Zry-4, these precipitates may play an important role at low H concentration (due to their preferential location respect to the hydrogen diffusion path) by producing deviations from the Zr–H diagram.

According to the Zr–H diagram, hydrogen has limited solubility in the Zr lattice, the terminal solid solubility (TSS), and, at higher concentration, the hydride phases precipitate [5,6]. The dependence of TSS with temperature can be obtained from useful empirical formulations. The morphology of hydride phases depends on the formation process where the cooling rate plays an important role. The precipitation of zirconium hydrides embrittles the zirconium alloy cladding reducing its ductility as well as its fracture toughness. It has been previously documented that this detrimental effect of hydrides causes premature fracture of nuclear fuel components in service [7].

Many authors [8–10] have found a ductility reduction in tensile tests, induced by H in Zr alloys; this reduction sometimes also reported as ductile-to-brittle transition [8]. Here, fracture mechanics is the most convenient methodology to study this behaviour since it not only characterises the toughness variation, but also gives a quantitative engineering magnitude that can be used in both design and in-service defect analysis.

A study of the detrimental effects of H on the elastic–plastic fracture toughness of a Zircaloy-4 commercial alloy at different temperatures is introduced in this work. Hydrogen precipitation mechanisms and their relationship with the toughness variation were also analysed aided by fracture surface observation. The existence of a ductile-to-brittle transition is discussed.

2. Material and experimental procedure

2.1. Material

All specimens were obtained from a Zry-4 rolled 6 mm thick plate. Fe, Cr, Sn and O in the proportion of 0.22:0.1:1.4:0.128 wt%, respectively, were the main alloying components in the Zr matrix; Sn and O in solid solution, and $Zr(Fe,Cr)_2$ in Laves phases precipitate form. The thermo-mechanical history of the plate included hot-rolling, annealing and final cold-rolling treatments. The final material microstructure was a α-Zry-4 fine equiaxed grains with a mean diameter of approximately 8 μm (Fig. 1). The main mechanical properties were ultimate tensile stress (σ_{UTS}) 522 MPa and 510 MPa, yield stress (σ_{ys}) 365 MPa and 460 MPa, and elongation (ε%) 27.8 and 26.6, measured at room temperature in the rolling and transverse direction respectively. The texture measurement revealed that the

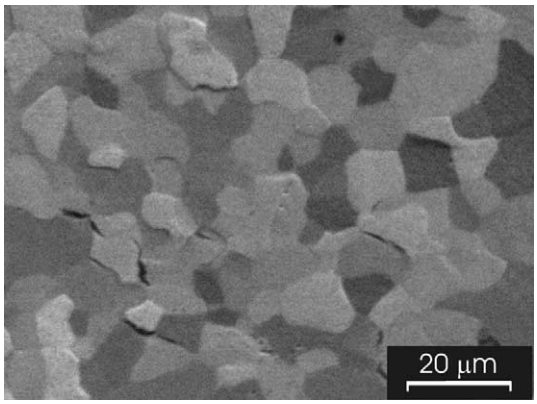

Fig. 1. Zry-4 microstructure, rounded grains with a mean diameter of 8 μm.

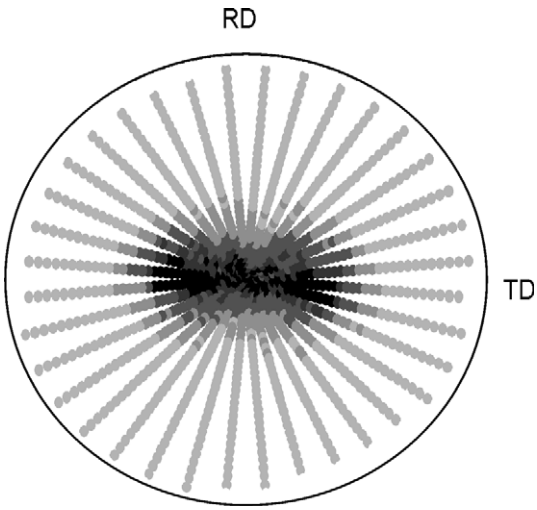

Fig. 2. Pole figure of basal plane.

{0002} poles were concentrated in the normal-transverse plane with a maximum about 36° from the normal direction (Fig. 2).

2.2. Hydrogen charging

To obtain samples with hydrogen content either above or below the H solubility limit, two charging methods were employed: cathodic and gaseous charging. Cathodic charging was carried out on pickled samples at room temperature in a 0.1 M KOH solution applying a current density of 10 mA/cm^2. To obtain a homogeneous hydride distribution after charging, the specimens were heated in argon atmosphere for 7 h at 720 K and then slowly cooled inside the furnace down to room temperature in order to allow hydrogen diffusion and precipitation. In this way, a strictly controlled although low final hydrogen content was obtained. Higher H

concentrations were obtained by gaseous charging under moderate hydrogen pressure and high temperature. In this case, the samples were placed in the reactor of a volumetric device where they were degassed in vacuum, then heated at least for 7 h at 720 K under a pure H atmosphere at a pressure of 2 bar, and finally they were slowly cooled down to room temperature inside the reactor. In this way H concentrations in the range of 400–2000 ppm were achieved.

Time and current density in the first technique, and time, temperature and H pressure in the second, are the experimental parameters that allow to obtain a wide range of final H content. A LECO™ hydrogen analyser was used to measure this value.

2.3. Specimens

Compact tension (CT) specimens were machined to final nominal dimensions: $W = 25.4$ mm and $B = 6$ mm with notches oriented transversely to the rolling direction. All specimens were fatigue pre-cracked to an a/W ratio between 0.45 and 0.55. Specimen dimensions followed ASTM E 1820-99 [11], but with $W/B = 4.23$ (outside of the standard specification) (Fig. 3).

2.4. Experimental procedure

All specimens were tested following ASTM E 1820-99 standard, evaluating the J–R curves by means of the single-specimen unloading compliance technique. After the test, the specimens were fatigue post-cracked to delineate the crack growth. The tests were performed at 293, 343, 393 and 473 K. Because the compliances were not measured on the load line, data corrections had to be made [12].

Specimens were heated by using two strip heaters. Temperature measurement and control were performed by means of a thermocouple with each wire welded to each specimen side, close to the crack tip. Therefore, only the zone close to the crack tip was heated. This methodology, introduced by McCabe and Landes [13], avoids heating the entire specimen plus the grip assembly, simplifying the experimental procedure.

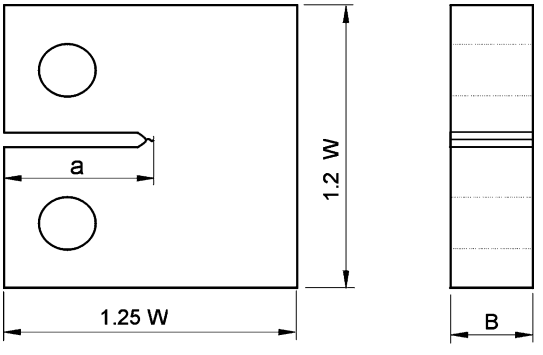

Fig. 3. Geometry of the tested CT specimens.

The stable crack growth initiation value (J_{IC}), and the J–R curve slope for 1 mm of stable crack growth ($\varphi_{1\ mm}$) were calculated when possible. J_C was evaluated for the few specimens exhibiting brittle fracture.

2.5. Metallographic and fractographic analysis

A standard procedure of mechanical polishing and chemical etching was carried out with a solution of 25 pct lactic acid, 25 pct H_2O, 46 pct HNO_3 and 4 pct HF to reveal the Zircaloy-4 microstructure, and a solution of 92 pct HNO_3 and 8 pct HF to reveal the Zr-hydrides distribution.

After the tests, one half of each specimen was observed through scanning electron microscopy (SEM) to study the fracture surface and hydride distribution, and to identify the micromechanisms responsible for the crack growth. The remaining halves were prepared for hydrogen content measurements.

2.6. Specimen size considerations

To ensure plane strain and J dominance conditions in the zone close to the crack tip, ASTM standards require that J values at crack growth initiation must meet:

$$\text{the smaller of } J \leqslant \frac{b \cdot \sigma_y}{20} \quad \text{or} \quad J \leqslant \frac{B \cdot \sigma_y}{20}, \tag{1}$$

where b is the remaining ligament ($W - a$), σ_y is calculated as the average of the 0.2% offset yield strength and the ultimate tensile strength, and B is the specimen thickness.

Considering the specimen thickness (6 mm) and the material yield stress, σ_y (443 MPa), from Eq. (1), the maximum valid J value was 133 kJ/m^2. Since some initiation values turned out higher than this J_{max}, they were termed J_Q in accordance with the standard.

3. Results

The hydrogen charge employed produced hydride precipitates of δ phase type, platelet shaped, oriented in planes parallel to the rolling direction, mainly at intergranular sites. The distribution and size of hydrides is influenced to a great extent by the cooling rate; for slow cooling rates the platelets are grouped in long bands [14] as it was well observed in this work (Fig. 4). The hydride distribution was also identified by employing a colorant treatment.

Fig. 5 shows the dependence of the load–displacement records on both H content and temperature. While the typical behaviour was ductile throughout stable crack growth mechanism, a few specimens exhibited

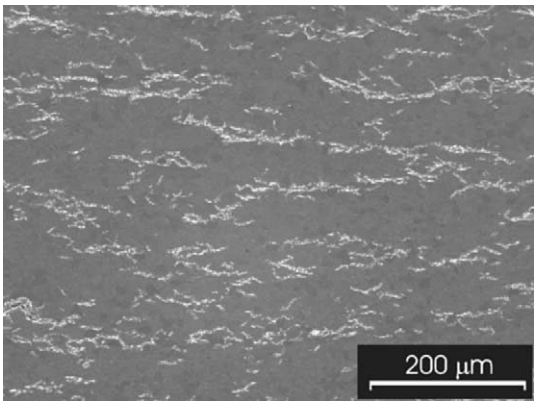

Fig. 4. Distribution of Zr-hydrides platelet.

sudden load drops at room temperature (RT) and high H content. Most instabilities corresponded to pop-in type (sudden load drops with compliance increase followed by stable crack growth mechanism); a small number of samples with high H content failed completely by brittle mode.

J–R curves at different temperatures for the as-received H content are shown in Fig. 6(a); J_{IC} and $\varphi_{1\ mm}$ values corresponding to these curves are plotted in Fig. 6(b). Fig. 7(a) and (b) plot the *J–R* curves, and the J_{IC} and $\varphi_{1\ mm}$ dependencies on H at room temperature respectively. Results of the whole tested range are shown in Fig. 8.

At low H content and regardless the test temperature, the fracture mechanisms observed were ductile by nucleation, growth and coalescence of microcavities (Fig. 9). At the highest temperatures, the fracture surface appearance was ductile with bigger dimples (Fig. 10). Some small brittle regions appeared when H content was about 300 ppm and were more frequent and larger as H was increased (Fig. 11).

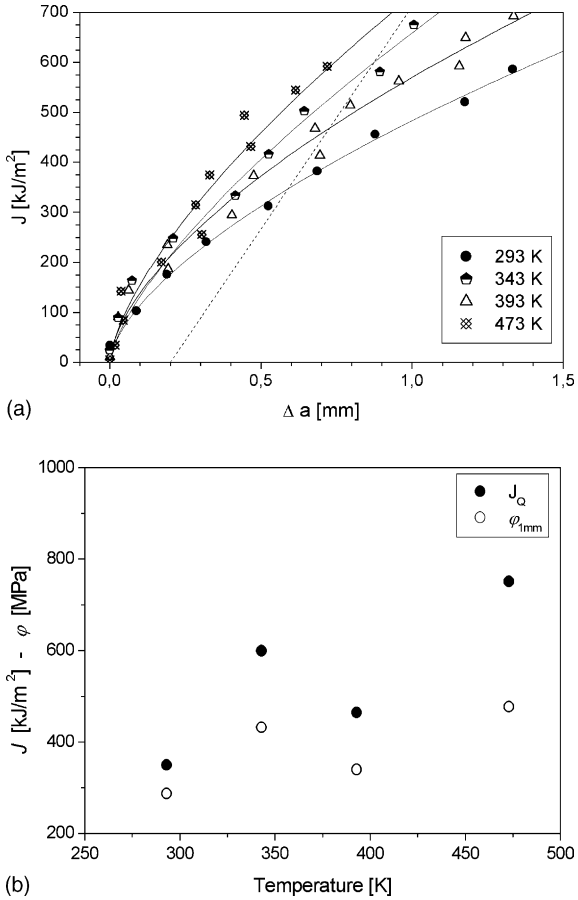

Fig. 6. Results at base H content as a function of the temperature. (a) *J–R* curves, (b) J_{IC} and $\varphi_{1\ mm}$.

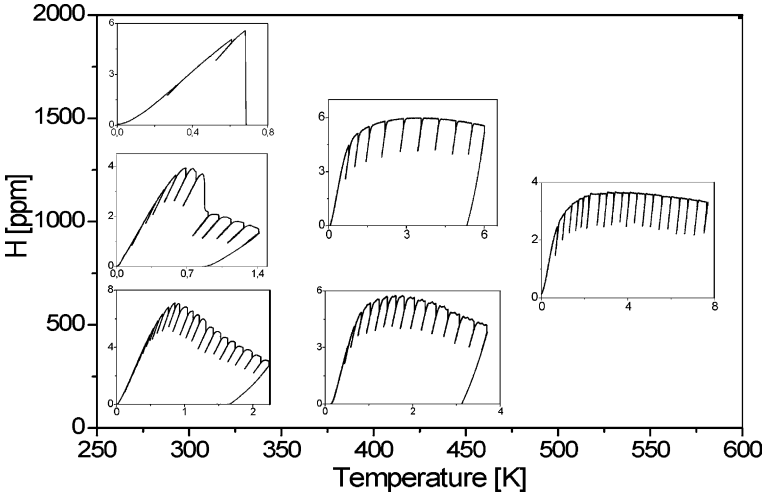

Fig. 5. *P* versus *v* records at different H content and temperatures showing the different behaviours observed (*P* [N] and *v* [mm]).

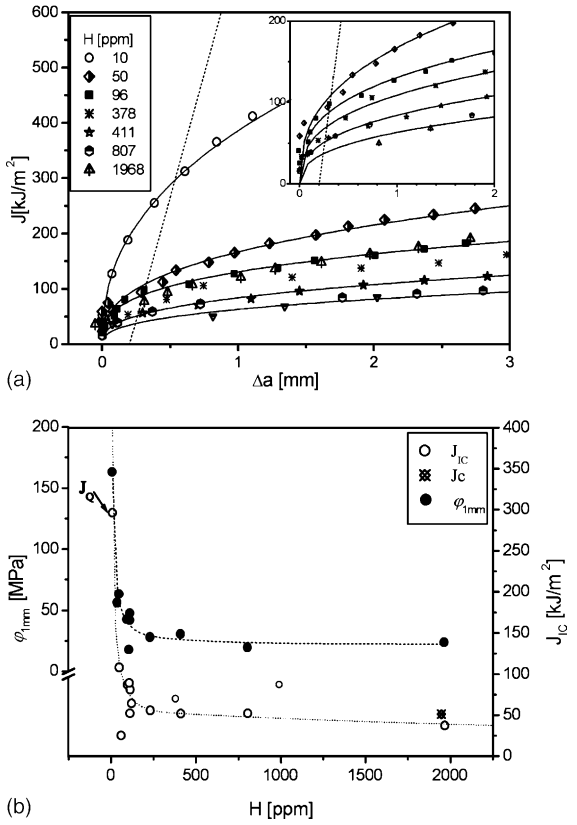

Fig. 7. Results at room temperature for different H content. (a) J–R curves, (b) J_{IC} and $\varphi_{1\ mm}$.

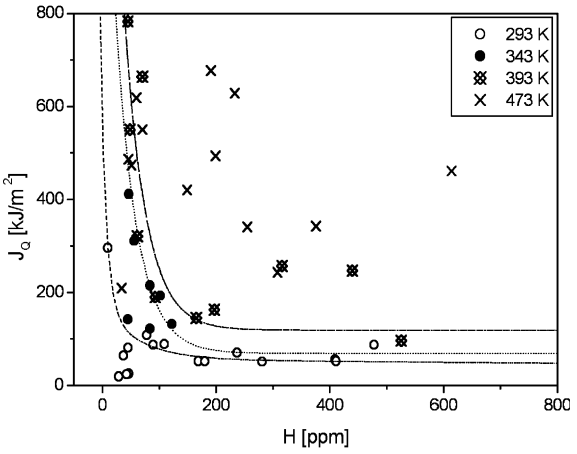

Fig. 8. J_{IC} versus H curves at different temperatures.

The fracture surfaces were also observed to study the density and composition of precipitates (mainly $Zr(Fe,Cr)_2$ Laves phases) and hydrided phases using the EDS facility of the SEM for the former, and its brittle appearance for the second (Fig. 12). Though Fe and Cr in precipitates could be clearly identified, the small precipitate sizes and the irregular fracture surface topographies prevented precipitate composition from being accurately measured. Previous report showed that the Cr/Fe ratio in Zry-4 can vary widely between 0.1 and 1.7 [15]. A correlation between global H content and density of precipitates in the fracture surfaces could be established; three different cases were identified:

1. At very low H contents (as-received material, H < 25 ppm) few $Zr(Fe,Cr)_2$ precipitates were observed on the fracture surface. No hydride phase could be identified, in agreement with the concentration value being lower than TSS.
2. When the H content increased, the density of $Zr(Fe,Cr)_2$ precipitates located on the fracture surface also grew. This behaviour was observed in H concentrations up to about 250–350 ppm, strongly suggesting that the precipitates guide the fracture path.

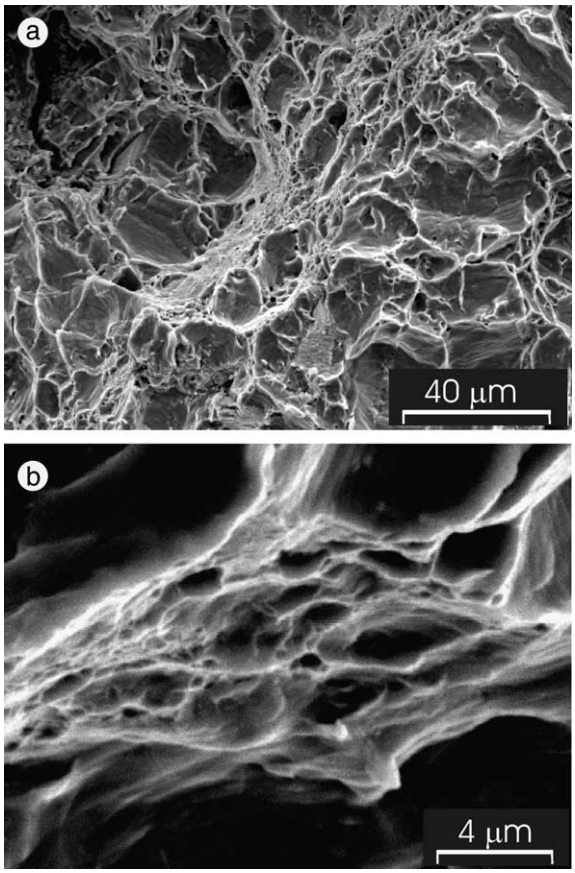

Fig. 9. Fractographies of one specimen with 50 ppm of H tested at room temperature, showing the typical ductile behaviour by nucleation and growth of voids.

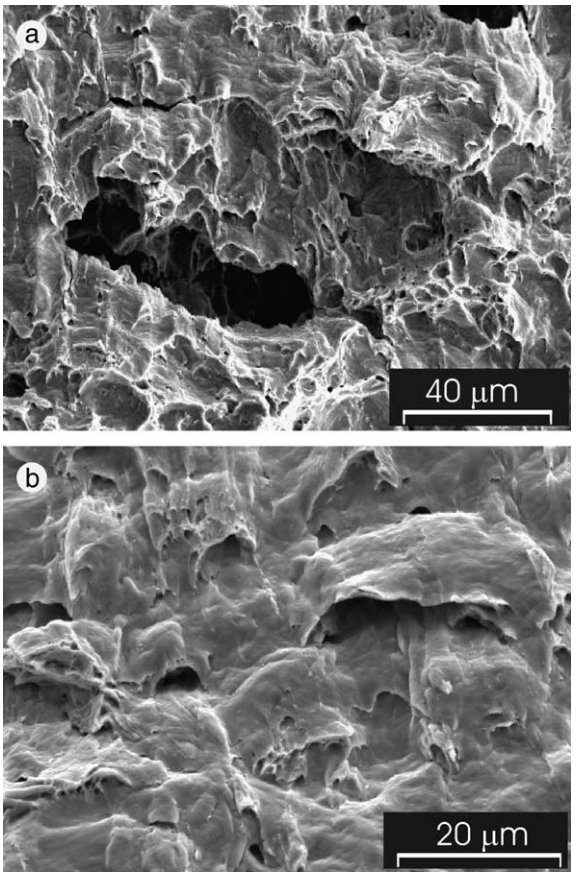

Fig. 10. Fracture surface of specimens tested at high temperature showing larger dimples; (a) 250 ppm H tested at 393 K and (b) 513 ppm H at 473 K.

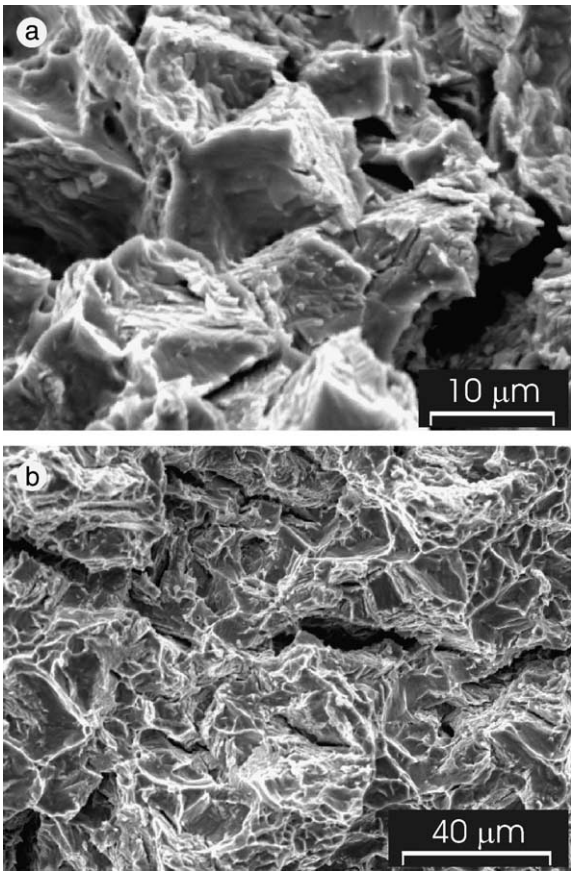

Fig. 11. Fractographies of specimens tested at room temperature where brittle regions can be observed, (a) 330 ppm and (b) 1900 ppm.

3. As the observed density of $Zr(Fe,Cr)_2$ precipitates on the fracture surface diminished at higher H contents, the region occupied by hydride phase grew indicating that this brittle phase determined the direction of crack growth and favoured the formation of a surface containing a mixed-mode fracture. Macroscopic behaviour was still ductile.

4. Discussion

As a consequence of the load–displacement records obtained (Fig. 5) including those that resulted in brittle fracture, elastic–plastic fracture mechanics was considered the adequate methodology to study hydrogen embrittlement over the concentration and temperature ranges analysed. Linear-elastic fracture mechanics was not employed to characterise fracture toughness in this work because its limits of applicability were violated.

Because of practical limitations, no observation of hydride precipitates could be performed during the fracture tests; however, post mortem measurements of the hydrogen concentration showed a homogeneous distribution within the volume. This fact cannot state whether redistribution may have not occurred in the highly stressed region near the crack tip during the tests, because it is well known that after the load removal the hydrides can be reoriented. The study of the influence of heterogeneous hydrogen distribution is the subject of work in progress.

Throughout the analysed temperature range, fracture behaviour was always macroscopically ductile at the as-received H content. Most combinations of temperature and H content proved a similar response. Brittle behaviour arose only at room temperature with the highest H content studied. Very large blunting values at the beginning of crack growth were obtained in tests performed at 473 K, making non-valid the calculated J_{IC}; so J_Q was reported instead. The tested specimens had the maximum thickness possible from the as-received material; therefore, thicker specimens could not be machined to test and then meet standard acceptable J_{IC}

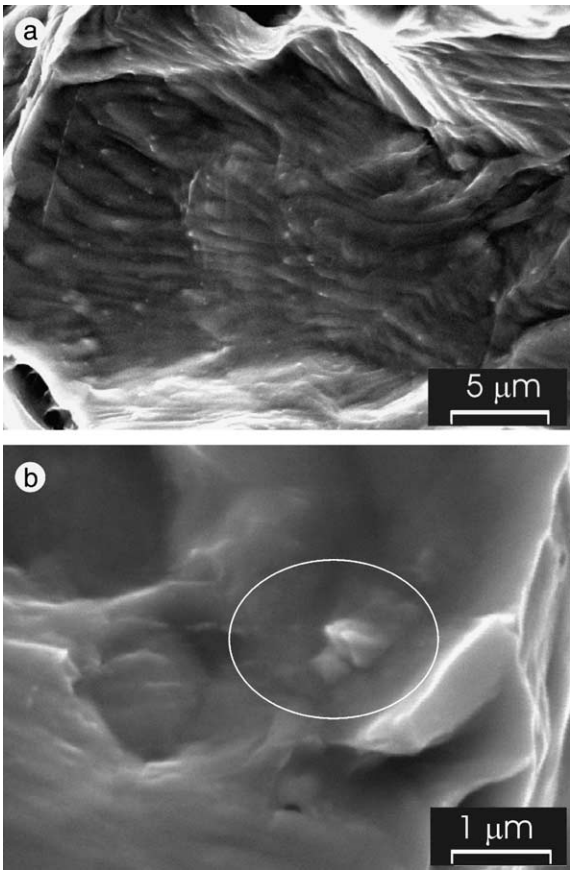

Fig. 12. (a) Fractography of a specimen with 100 H ppm tested at room temperature where a high number of $Zr(Fe,Cr)_2$ precipitates (white dots) can be observed, (b) magnification of one precipitate.

values. *J–R* curves could not be determined at temperatures around 523 K and higher because the crack blunting was too large and no stable crack growth was present during the tests. Although J_Q values stand out of the standards and are not considered a material property, they contribute important information about the toughness tendencies.

Fig. 7(b) shows a clear trend in values measured at constant temperature: a high susceptibility of the material toughness for small H variations at low H contents, but soft dependence for H concentrations higher than 250 ppm. This behaviour can be fitted with an exponential decay function. For higher temperatures, the curve displaces towards higher toughness values (Fig. 8). The toughness reduction associated to H was always greater than the improvement caused by temperature augment; that is, the increase of temperature restored only a fraction of the degradation caused by H.

'Anomalous' *J* values were obtained at about 343 K, where a relative maximum in fracture toughness was present. Initiation and curve slope values were higher than expected (Fig. 6). This behaviour could be due to Dynamic Strain ageing effect. Several authors [16,17] have reported some hardening peaks in the yield stress in tensile tests of Zr at different temperatures. This change in the tensile behaviour must undoubtedly have consequences in the toughness values.

The expression 'ductile-to-brittle transition' generally refers to a change in both micromechanisms and macroscopic behaviour. Reported Zry-4 results refer to a ductile-to-brittle transition by analysing tensile parameters, specifically elongation and reduction of area [9] [10]. Bai et al. say: 'The existence of ductile-to-brittle transition for high C_H is confirmed by the reduction of area measurements' [8], while Grange et al. conclude 'The brittle–ductile transition may be interpreted as a transition in the hydride morphology and site of precipitation, probably in direct relationship to the precipitation mechanism' [18]. Although the macroscopic behaviour was generally ductile with stable crack growth, a reduction on *J* values as temperature diminished and H increased was observed. Only for tests at room temperature in samples with high H contents, *P* versus *v* records showed instabilities (pop-in or full brittle fracture for the highest H content); therefore, they could be associated with a transition in macromechanisms (Fig. 8).

For low H content the fracture mechanisms observed in the SEM were ductile by nucleation, growth and coalescence of microcavities, while some brittle regions appeared when H content was increased. Large longitudinal oriented cracks, parallel to the specimen face, were observed in some specimens. These observations are in agreement with Grange's report [18] on the change in micromechanisms when H content increases.

Since the H content studied ranged from 10 to 2000 ppm, and taking into account that the TSS of hydrogen in Zr varied from 0.01 to 10 wt. ppm over the 293/473 K range [19,20], the experiments involved a material with composition located in the two-phase region of the equilibrium Zr–H phase diagram, i.e. a Zr-hydride phase nucleated (Fig. 4). Because of the favourable location of $Zr(Fe,Cr)_2$ precipitates in the grain boundaries, their affinity to form hydride phases and the higher diffusion coefficient of H in grain boundaries than in the grains, the reaction of the precipitates with H could play an important role in the fracture process.

The fractographic observations showed a close relationship between H content and $Zr(Fe,Cr)_2$ precipitates in the crack path. The explanation could be as follows: during absorption, H diffuses preferentially through grain boundaries and firstly reacts with $Zr(Fe,Cr)_2$ precipitates forming hydrides. This hydriding process embrittles the precipitates, increases the precipitate volume and, consequently, generates a stress–strain field that favours the crack growth through it. At low and medium

H content (less than 250 ppm), these precipitates could act as dimple nucleation sites. At higher H content, the density of a Zr-hydride phase is higher and first competes with hydrided $Zr(Fe,Cr)_2$ precipitates, then dominates them in the path selection for crack growth. As it can be seen in Fig. 11, brittle regions are more frequent and larger as H content increases; such regions correspond to the crack growing through the Zr-hydride precipitates.

At medium H content the hydride phase nucleus are small, the crack growing macroscopically in a stable manner, although microscopically in a brittle mode through the hydrides (ZrH) and in a ductile way through the matrix. When the hydrides are massive enough, the typical pop-in behaviour can be observed, and corresponds to a sudden crack growth through the hydrides with a posterior crack arrest at the matrix. If the hydrides are large enough, the matrix can no longer arrest the growing crack, producing a fully unstable fracture. So, the whole influence of the hydrogen on the fracture process can be understood in terms of competition between the original Laves phase precipitates that were hydrided versus Zr-hydrides and the respective influence of their strain fields at medium H content. For higher H contents, the Zr-hydrides dominate the process, beginning with a ductile fracture while the ZrH precipitates are small, through a mixed micromode of fracture with tiny brittle regions, ending with brittle fracture when the hydrides are massive enough.

The J_{IC}–H curves (Figs. 7(b) and 8) show a fracture toughness steep reduction in the hydrogen range up to 250 ppm approximately; these H contents correspond to those where the fracture surface shows the highest $Zr(Fe,Cr)_2$ precipitate concentrations. At higher H content, a gradual toughness reduction was observed and could be related with the range where the Zr-hydrides dominate the fracture process. An interesting aspect to highlight is that the great toughness reduction at low H contents happens exclusively within ductile macromechanisms, whilst there are no important changes in fracture toughness at high H values involving a transition in macroscopic mode of fracture.

5. Conclusions

The main behaviour observed was ductile and only a few specimens, with very high H content, failed by brittle mode when tested at room temperature. At higher temperatures the *J–R* curves raised, increasing both initiation and resistance to growth values. At room temperature, the *J–R* curves dependence on H content were fitted with an exponential decay for the initiation values as well as for the slope ones. When the temperature grows, the values of J_{IC} and $\varphi_{1\ mm}$ increased retaining the functional dependence on H. Here, a 'ductile-to-brittle transition', in the sense of a change in macroscopic behaviour, was not related to the changes in toughness values. Either pop-in or brittle fractures were observed only at room temperature and in samples with the highest hydrogen content in the studied range.

The fracture micromechanisms in hydrided Zry-4 are strongly dependent on the hydrogen content. For low H content, ductile fracture occurs by formation and growth of voids. For the specimens with high H content brittle areas appeared, indicating fracture through hydrides. Three stages were identified after correlating H content with precipitates density in the fracture surface.

Acknowledgements

To CNEA (Atomic Energy National Commission) and CONICET (National Council of Scientific and Technological Research) for having supported this project.

References

[1] B.F. Kammenzind, D.G. Franklin, R.H. Peters, W.J. Duffin, ASTM STP 1295 (1996) 338.
[2] J.C. Clayton, ASTM STP 824 (1984) 572.
[3] J.C. Clayton, ASTM STP 1023 (1988) 266.
[4] E. Zuzek, J.P. Abriata, A. San Martín, F.D. Manchester, in: F.D. Manchester (Ed.), Hydrogen–Zirconium, Phase Diagrams of Binary Alloys, 2000, p. 309.
[5] A. Sawatzky, J. Nucl. Mater. 2 (1960) 62.
[6] J.J. Kearns, J. Nucl. Mater. 22 (1967) 292.
[7] C.K. Chow, L.A. Simpson, ASTM-STP 918 (1986) 78.
[8] J.B. Bai, C. Prioul, C. François, Metall. Mater. Trans. A 25A (1994) 1185.
[9] S.C. Lin, M. Hamasaki, Y.D. Chuang, Nucl. Sci. Eng. 71 (1979) 251.
[10] J.H. Huang, S.P. Huang, C.S. Ho, Scr. Metall. Mater. 28 (1993) 1537.
[11] ASTM, 1999, Standard Test Method for Measurement of Fracture Toughness, ASTM E 1820-99, Annual Book of ASTM Standards, vol. 03.01, ASTM, 1999, p. 972.
[12] J.E. Perez Ipiña, Eng. Fract. Mech. 36 (5) (1990) 797.
[13] D.E. McCabe, J.D. Landes, ASTM STP 803 (II) (1983) 352.
[14] K.W. Lee, S.I. Hong, J. Alloys Compd. 346 (1–2) (2002) 302.
[15] D. Arias, T. Palacios, C. Turrillo, J. Nucl. Mater. 148 (1987) 227.
[16] V. Ramachandran, R.E. Reed-Hill, Metall. Trans. 1 (1970) 2105.
[17] A.M. Garde, E. Aigeltinger, B.N. Woodruff, R.E. Reed-Hill, Metall. Trans. A 6A (1975) 1183.
[18] M. Grange, J. Besson, E. Andrieu, Metall. Mater. Trans. A 31A (2000) 679.
[19] D.L. Douglass, At. Energ. Rev., IAEA Suppl. 1971 (1971) 160.
[20] C.E. Ells, J. Nucl. Mater. 28 (1968) 1289.